Influence of dissolved black carbon on the aggregation and deposition of polystyrene nanoplastics

Comparison with dissolved humic acid

Xu, Yanghui; Ou, Qin; He, Qiang; Wu, Zhengsong; Ma, Jun; Huangfu, Xiaoliu

DOI
10.1016/j.watres.2021.117054

Publication date
2021

Document Version
Final published version

Published in
Water Research

Water Research 196 (2021) 117054

Contents lists available at ScienceDirect

Water Research

journal homepage: www.elsevier.com/locate/watres

Influence of dissolved black carbon on the aggregation and deposition of polystyrene nanoplastics: Comparison with dissolved humic acid

Yanghui Xu[a,b,§], Qin Ou[a,§], Qiang He[a], Zhengsong Wu[a], Jun Ma[c], Xiaoliu Huangfu[a,*]

[a] Key Laboratory of Eco-environments in Three Gorges Reservoir Region, Ministry of Education, Faculty of Urban Construction and Environmental Engineering, Chongqing University 400044, China
[b] Section of Sanitary Engineering, Department of Water Management, Faculty of Civil Engineering and Geosciences, Delft University of Technology, Stevinweg 1, 2628 CN Delft, the Netherlands
[c] State Key Laboratory of Urban Water Resource and Environment, School of Municipal and Environmental Engineering, Harbin Institute of Technology 150001, China

ARTICLE INFO

Article history:
Received 14 December 2020
Revised 11 March 2021
Accepted 13 March 2021
Available online 15 March 2021

Keywords:
Dissolved black carbon
Dissolved humic acid
Nanoplastics
Aging
Aggregation
Deposition

ABSTRACT

Dissolved black carbon (DBC), widely found in soil and water environments is likely to affect the transport of nanoplastics in aquatic environments. The aggregation and deposition behaviors of fresh and aged polystyrene nanoplastics (PSs) with and without DBC in NaCl solution were investigated by time-resolved dynamic light scattering (DLS) and quartz crystal microbalance with dissipation monitoring equipment (QCM-D) techniques. The results suggest that DBC can screen the surface charges of PSs by interacting with PSs through hydrogen bonding, hydrophobic interactions and π-π interactions, although they were negatively charged. DBC promoted the aggregation of PSs under relatively low ionic strengths, and it minimally affected the stability of PSs under high ionic strength. Deposition experiments showed that both DBC in salt solution and DBC adsorption on silica surface facilitated the deposition of fresh PSs while HA inhibited both deposition processes. After aging, PSs were more stable, and the effects of DBC and HA were weakened. This study investigated the influence mechanism of DBC on the aggregation and deposition behaviors, which provides new insights into the stability and transport of PSs in complex aquatic environments.

1. Introduction

The extensive usage of plastic materials results in the excess release into the environment, which constitute up to 60–80% of marine litter (Eerkes-Medrano, Thompson et al. 2015, Erni-Cassola, Gibson et al. 2017, Alimi, Farner Budarz et al. 2018). After chemical degradation, biodegradation, photodegradation, thermal degradation, and mechanical abrasion, these plastics can are continuously broken down to form microplastics (MPs) with sizes of 0.1 mm–5 mm or nanoplastics (NPs) with sizes of < 100 nm (Alimi, Farner Budarz et al. 2018, Mao, Ai et al. 2018, Xu, He et al. 2019, Mao, Li et al. 2020, Mao, Li et al. 2020). NPs might be discharged from wastewater treatment plants into the environment, or migrate into rivers and oceans via atmospheric deposition or overland runoff (Bergami, Pugnalini et al. 2017, Besseling, Quik et al. 2017, Cai, Hu et al. 2018). After exposure to aquatic environments, NPs can be ingested by a wide range of aquatic organisms including mammals (Besseling, Foekema et al. 2015), fish (Alomar and Deudero 2017) zooplankton (Cole, Lindeque et al. 2016), and phytoplankton (Mao, Ai et al. 2018), causing cytotoxicity and metabolic disorders. NPs can undergo various transformations, including aggregation, deposition, aging, or degradation (Eerkes-Medrano, Thompson et al. 2015, Aller 2016, Besseling, Quik et al. 2017, Alimi, Farner Budarz et al. 2018, Enfrin, Dumee et al. 2019), which are closely associated with their fate and toxicity in environments. Previous studies have investigated the environmental behavior of NPs in soils and waters (Summers, Henry et al. 2018, Liu, Hu et al. 2019, Mao, Li et al. 2020, Wang, Zhao et al. 2021). NPs exhibit high colloidal stability under common water conditions (Wu, Jiang et al. 2019, Yu, Shen et al. 2019, Shams, Alam et al. 2020, Wang, Zhao et al. 2021). Mao et al. reported that the critical coagulation concentration (CCC) of polystyrene (PS) NPs was 590 mM for Na^+ and 74 mM for Ca^{2+} (Mao, Li et al. 2020). Similarly, Shams et al. also concluded that CCC values of PSs were 10 mM for $CaCl_2$, 800 mM for NaCl and 25 mM for $MgCl_2$ (Shams, Alam et al. 2020). In addition to the homoaggregation behavior of NPs in synthetic and natural

* Corresponding author.
E-mail address: hfxl-hit@163.com (X. Huangfu).
§ The authors contribute equally to this work.

https://doi.org/10.1016/j.watres.2021.117054
0043-1354/

waters, heteroaggregation with natural colloids and nanoparticles also plays an important role in their transport and bioavailability in aquatic systems (Long, Paul-Pont et al. 2017, Cai, Hu et al. 2018, Oriekhova and Stoll 2018, Liu, Hu et al. 2019). A certain concentration of negatively charged alginate and Fe_2O_3 can destabilize PSs with amino functional groups due to charge neutralization, while further increasing the alginate and Fe_2O_3 concentrations could induce charge inversion, thereby reducing the aggregate sizes (Oriekhova and Stoll 2018). Extracellular polysaccharides promote the interactions of PS MPs and marine phytoplankton, resulting in species-specific heteroaggregation (Long, Paul-Pont et al. 2017). Large suspended sediment with sizes of 100–500 mm significantly increased the aggregation and settling of PSs with an average diameter of 100 nm while the presence of humic acid (HA) decreased the heteroaggregation between suspended sediment and PSs because of steric repulsion (Liu, Hu et al. 2019). Although previous studies have provided some insights into the heteroaggregation behaviors of NPs, the mechanisms of heteroaggregation between NPs and natural colloids as well as nanoparticles require further investigation.

Black carbon (BC), an important carbon component of soil and sediment systems, has attracted widespread attention in agricultural and environmental fields because of its roles in many related biogeological processes, including the transport of contaminants, carbon cycling, and soil conditioners (Ouyang, Zhao et al. 2016, Qu, Fu et al. 2016). With the rainfall and irrigation, BC can release a water-soluble fraction called dissolved BC (DBC) into aquatic environments (Xu, Wei et al. 2017), which accounts for approximately 10% of dissolved organic carbon in rivers and 2% in oceans globally (Hopkinson and Vallino 2005, Dittmar and Paeng 2009, Dittmar, de Rezende et al. 2012, Rudolf Jaffé, Yan Ding et al. 2013). In addition, particulate or nanoparticulate BC might form because of the physical disintegration of BC after aging and weathering in the environment (Qian, Zhang et al. 2016). In China, particulate BC accounted for 13 ± 0.9% and 22 ± 11% of the particulate organic carbon pools in the Changjiang and Huanghe rivers, respectively (Xu, Xue et al. 2016). Previous studies have suggested that DBC exhibits high stability under environmental conditions (Xu, Wei et al. 2017). Xu et al. found that DBC is hard to aggregate even at 800 mM Na^+ or Mg^{2+} solutions because of the strong hydration force (Xu, Wei et al. 2017). The CCC values of DBC produced at 400 °C and 700 °C were 700 and 140 mM for Na^+ (Lian, Yu et al. 2019). In addition, as DBC has abundant aromatic domains and oxygen-containing functional groups such as carboxyl (−COOH) and hydroxyl (−OH) groups, it might exhibit strong affinity to environmental pollutants and soil matrices (Harvey, Herbert et al. 2011, Yao, Gao et al. 2014, Lian and Xing 2017, Alam, Gorman-Lewis et al. 2018, Luo, Chen et al. 2019, Xu, Ou et al. 2020). Considering its high mobility and reactivity, DBC is expected to have an impact on the transport and fate of associated contaminants, such as NPs.

Owing to their high surface-to-volume ratio and high surface hydrophobicity, NPs exhibit strong affinities toward a range of hydrophobic organic chemicals such as polychlorinated biphenyls (PCBs), polycyclic aromatic hydrocarbons (PAHs) and perfluorinated surfactants (Chua, Shimeta et al. 2014, Velzeboer, Kwadijk et al. 2014, Huffer and Hofmann 2016, Liu, Fokkink et al. 2016, Liu, Ma et al. 2018). PSs have higher adsorption ability to PCBs than polyethylene MPs because of the higher aromaticity and surface-volume ratio of PSs (Velzeboer, Kwadijk et al. 2014). The π–π interactions between PAHs and the aromatic polymer PS contributed to the high and nonlinear adsorption (Liu, Fokkink et al. 2016). With adequate aromatic components, DBC might strongly adsorb to the surface of NPs via hydrophobic interactions and π–π interactions, thereby impacting the transport of NPs. However, limited research has investigated the impact of DBC on the transport of PSs in aquatic environments.

In this study, to investigate the effect of DBC on the stability and transport of PSs, the aggregation and deposition behaviors of primary and aged PSs with and without DBC or HA were studied. First, the DLS method was applied to study the aggregation behavior of the aggregation kinetics of PSs with and without DBC from various sources. Moreover, the QCM-D technique was utilized to examine the deposition of individual PSs on the SiO_2 surface, the co-deposition behavior of DBC and PSs on SiO_2 surface, and the deposition of PSs on the DBC-modified SiO_2 surface.

2. Materials and methods

2.1. Materials

A PS stock solution (aqueous suspension) with a diameter of 0.05–0.1 μm was purchased from Macklin Biochemical Co., Ltd (Shanghai, China). The stock solution had a particle concentration of 2.5% w/v (i.e., 25 g/L) of PSs without surface modification. Prior to the experiments, the PS suspension was prepared by diluting the stock solution with ultrapure water to obtain 40 mg/L PS. A final PS concentration of 10 mg/L was used in all experiments, which was selected as a representative nanoplastic concentration commonly applied in previous studies (Liu, Hu et al. 2019, Yu, Shen et al. 2019, Liu, Huang et al. 2020, Wang, Zhao et al. 2021).

The PS aging experiments were conducted in an aging chamber equipped with a UV lamp (UVC-254 nm, 15W). A 250 mL suspension of 40 mg/L PS was added to a quartz vial and a UV lamp was inserted into the reactor. The sample was exposed to UV light for either 12 h or 24 h and stirred constantly to ensure uniform exposure. The unaged samples and PSs aged for 12 h and 24h, named PS_0, PS_{12} and PS_{24}, respectively, were stored at 4–8 °C before use.

DBC originating from biochar was prepared by an ultrasonic method (Luo, Xu et al. 2015, Xu, Wei et al. 2017); the detailed procedure is presented in Text S1 of the Supplementary Material. Different types of DBC were prepared using maize straw biochar (pyrolyzed at 500 °C and 300 °C), wood and rice straw biochar (pyrolyzed at 500 °C) as raw materials, termed MS5, MS3, WO, RS, respectively. HA, was purchased from Sigma-Aldrich (CAS1415-93-6) and used as a representative aquatic humic substance. The total organic carbon (TOC) content of DBC and HA solutions was measured to determine their concentrations. The MS5, MS3, WO, RS and HA stock solution with a concentration of 10 mg C/L were stored at 4–8 °C prior to the experiments. According to published values of dissolved organic carbon (DOC) and DBC (0.001–3.7 mg C/L) in aquatic environments (Ding, Cawley et al. 2014, Wagner, Jaffé et al. 2018), the experimental concentrations of DBC and HA were selected as 2 mg/L.

2.2. Characterization of PSs and DBC

The structural properties and functional groups of unaged and aged PSs, DBC, and HA samples were determined by Fourier transform infrared spectroscopy (FTIR). FTIR analysis was performed using the KBr tablet method with wavenumbers ranging from 400 to 4000 cm^{-1}. X-ray photoelectron spectroscopy (XPS) was used to characterize the surface chemical compositions of these samples (Qu, Fu et al. 2016). The XPS measurements were performed with a PHI 5000 Versaprobe system (ULVAC-PHI, Japan) using monochromatized Al Kα radiation ($h\nu$ = 1486.6 eV). All samples were freeze-dried before FTIR and XPS characterization. The hydrodynamic sizes and zeta potentials of PSs were measured at 25 °C via dynamic light scattering (DLS) using a Zetasizer Nano ZS90 (Malvern Instruments, UK) operated with a HeNe laser at a wavelength of 633 nm and a scattering angle of 90°. To determine effect of DBC and HA on the surface charge of PSs, the zeta potentials of

PSs with or without DBC and HA were measured over a range of NaCl concentrations at pH 7 (adjusted by using 0.1 M NaCl and HCl). Each sample was measured in triplicate, with 10 runs per measurement.

2.3. Aggregation kinetics measurements

The aggregation kinetics of PSs under various solution were determined by time-resolved DLS measurements using a Malvern Zetasizer instrument (Nano ZS, Malvern, UK) with a He–Ne laser at a wavelength of 633 nm and a fixed scattering angle of 90° (Xu, Ou et al. 2020). Prior to each measurement, the PS samples were sonicated in a water bath for 15 min. During the aggregation measurements, 1.5 mL of the PS suspension was added to the DLS polystyrene cuvette, followed by the addition of 1.5 mL of the prepared NaCl solution. For the aggregation processes in the presence of DBC and HA, the PSs, DBC, HA and NaCl solutions were mixed in a certain proportion. The final concentrations of PSs and DBC were 10 mg/L and 2 mg TOC/L, respectively. The time-resolved DLS measurements continuously monitored the average hydrodynamic diameter of PSs every 30 s for 30 min, with no delay between measurements. All measurements were conducted in triplicate to increase statistical power for data analysis.

The aggregation kinetics of PSs in the initial stage were evaluated by measuring the initial rate of change in hydrodynamic size (D_h) over time t. The initial aggregation rate constant (k) was proportional to the initial rate of increase in D_h and inversely proportional to the initial PS concentration of PSs in the suspension (M_0) (Equation (1)) (Jiang, Raliya et al. 2016).

$$k \propto \frac{\left(\frac{dD_h(t)}{dt}\right)_{t\to 0}}{M_0}, \tag{1}$$

The initial rate of the linear increase of D_h for PSs with time ($dD_h(t)/dt$) was determined from t = 0 to the time when D_h reached $1.5D_{h0}$. The value of $dD_h(t)/dt$ was calculated using a linear least squares regression analysis. The attachment efficiency (α) applied to characterize the stability of PSs was calculated by normalizing k under different solution conditions to k_f under fast aggregation conditions (Liu, Legros et al. 2013).

$$\alpha = \frac{k}{k_f} = \frac{\left(\frac{dD_h(t)}{dt}\right)_{t\to 0}}{\left(\frac{dD_h(t)}{dt}\right)_{t\to 0,fast}}, \tag{2}$$

2.4. Deposition experiments

The PS deposition experiments in aquatic solution were performed using a QCM-D D300 system (Q-Sense AB, Gothenburg, Sweden). The selected silica (SiO_2, QSX 303) surface purchased from Q-sense AB was a representative environmental surface. QCM-D experiments were conducted to monitor changes in the frequency (Δf) of a 5 MHz AT-cut quartz sensor crystal. The QCM sensors were cleaned according to the standard cleaning protocols recommended by the Q-sense (Text S2) prior to each deposition experiment. The flow rate of the solution was controlled at 0.15 mL/min, and the experiment was performed at 25°C.

To investigate the effect of DBC on the deposition behavior of PSs on silica surfaces. The deposition of individual PSs on the SiO_2 surface, the co-deposition behavior of DBC and PSs on the SiO_2 surface, and the deposition of PSs on the DBC-modified SiO_2 surface were examined. In each deposition experiment, the QCM-D system was first pre-equilibrated with the desired salt solution to obtain a stable baseline at 0.15 mL/min. For the first case, the prepared PS suspension (10 mg/L) in desired salt solution was then injected into the crystal chamber to obtain the frequency shift curve. For the co-deposition process, PS suspension (10 mg/L) with 2 mg C/L DBC or HA in the desired salt solution was injected to obtain the frequency shift curve. For the last case, DBC or HA samples (2 mg C/L) were first injected to obtain a stable baseline, then the desired salt solution was injected to remove the unabsorbed DBC or HA. Finally, the PSs in the desired salt solution were injected.

The continuous increase in the mass of the deposited PSs or DBC (Δm) can lead to a shift in the resonance and overtone frequencies (Δf), described by the Sauerbrey relationship:

$$\Delta m = -\frac{C\Delta f_n}{n}, \tag{3}$$

Where n is the overtone number (n = 3 in this study) and C is the crystal constant (17.7 ng/Hz/cm^2 when f = 5 MHz).

The initial deposition rate (r_D), quantified by the initial shift of the normalized frequency at a given period, was obtained to determine the deposition kinetics (Chen and Elimelech 2006).

$$r_D = \frac{d\Delta f_3}{dt}, \tag{4}$$

3. Results and discussions

3.1. Characterization of PSs and DBC

The particle size, morphology, and hydrodynamic size of primary PSs and DBC were determined by SEM and DLS measurements. The SEM images showed that the average diameter of the PSs was 50 nm, exhibiting a regular spherical morphology (Fig. S1). DLS measurement showed the average hydrodynamic size of PSs was 117.8 ± 5.7 nm. DLS was further used to determine the zeta potential of the PSs (Fig. S2). The fresh PSs had strong negative surface charge with a ζ-potential of 44.4 ± 1.3 mV as measured at 10 mM NaCl and pH 7 (Fig. S2), which indicated that the fresh PSs were very stable (Liu, Hu et al. 2019, Liu, Huang et al. 2020). After UV radiation, the ζ-potential of PSs barely changed (41.4 ± 3.5 mV for PS_{12} and 43.3 ± 1.8 mV for PS_{24} at 10 mM NaCl and pH 7) (Fig. S2), which was similar to the results of previous studies (Liu, Hu et al. 2019). The hydrodynamic size of fresh PSs decreased to 98.1 ± 4.1 and 70.9 ± 4.4 nm at 12 and 24 hours after UV irradiation, respectively (Fig. S3). FTIR and XPS were further used to characterize the functional groups and surface elemental composition of fresh and aged PSs (Fig. 1, S4 and Table S1). For fresh PSs, typical adsorption peaks were identified at 1500 and 1649 cm^{-1} that corresponded to C=C stretch of aromatic ring and alkene, respectively (Liu, Hu et al. 2019, Mao, Li et al. 2020). Aromatic C–H bending contributed to the adsorption peaks at 698 and 831 cm^{-1} (Luo, Chen et al. 2019). For PS_{12} and PS_{24}, the broad adsorption peaks of C=O stretching (1600–1755 cm^{-1}) implied the formation of hydrophilic groups after ageing. Moreover, the polarity indexes [(O+N)/C] of PS_0, PS_{12}, and PS_{24} were 0.07, 0.11, and 0.18, respectively (Table S1), suggesting aged PS contained more polar functional groups (Lian, Yu et al. 2019, Liu, Hu et al. 2019).

The SEM images showed that the morphology of DBC was irregular, and the particle size was not uniform or definite (Fig. S1). All DBCs were negatively charged and the ζ-potential of DBC generally followed WO > RS > MS5 > MS3 (Fig. S5). FTIR was used to analyze the surface functional groups of the DBC (Fig. 1). The strong absorbance at 3361, 1622, 1400, 1251, and 1120 cm^{-1} of MS5 suggest that it contained O-containing functional groups such as C–O–C, –OH, and C=O groups (Lian, Yu et al. 2019). Additionally, the unsaturated aromatic C=C stretching at 1560 cm^{-1} and aromatic C–H bending (625–900 cm^{-1}) indicated the abundance of aromatics (Luo, Chen et al. 2019). Similarly, FTIR also indicated that the presence of O-containing functional groups and aromatic components in MS3, WO, RS and HA (Fig. 1). The polarity indexes of MS5, MS3, WO, RS and HA were 0.45, 0.50, 0.37, 0.42, 0.45, respectively, and almost followed WO < RS < MS5 ≈ HA < MS3 (Table S1).

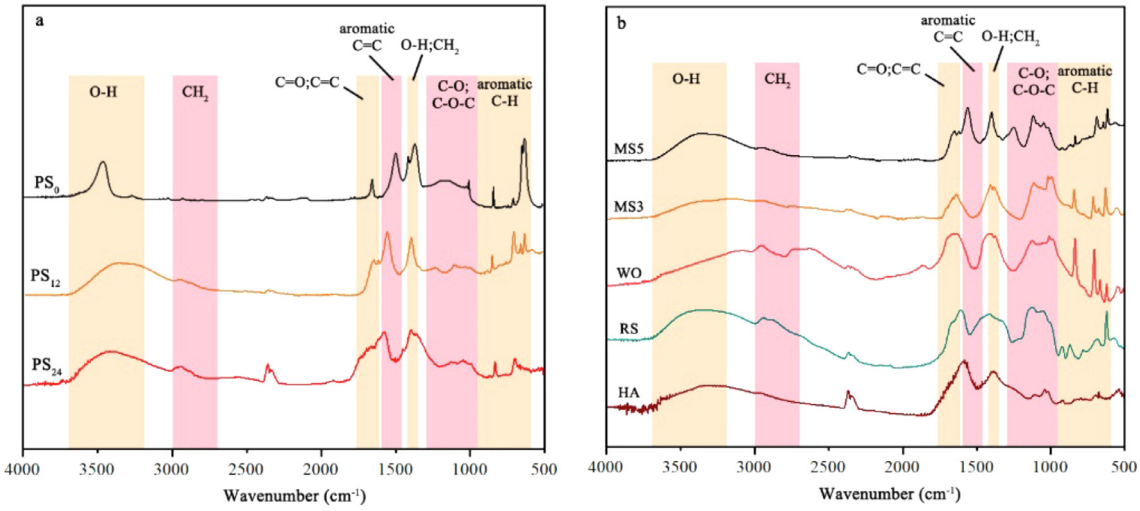

Fig. 1. The FTIR spectra of samples. (a) fresh and aged PSs, (b) DBC and HA.

Additionally, the ζ-potential of PSs in the presence of MS5, MS3, WO, RS and HA in a range of NaCl concentrations were measured (Fig.S2). Interestingly, the addition of a certain amount of DBC reduced the ζ-potential of PSs. Both the DBC and PS were negatively charged (Fig. S5), but a decrease in the negative charge on the PSs was observed in this study. Owing to the abundance of O-containing groups and aromatic constituents of DBC, other interactions such as hydrogen-bonding, hydrophobic and π-π interactions may overcome electrostatic repulsion, resulting in the adsorption of DBC onto the PS surface. Thus, the partial charge of PSs was shielded by BC molecule distributed unevenly on the PS surface. The ζ-potential increased more when the concentration of added DBC (MS5) was higher, which indicated the spatial shielding of the surface charge was enhanced. In addition, the ζ-potential of PSs in the presence 2 mg C/L MS5, MS3, WO, RS almost followed WO > RS > MS5 > MS3 (Fig. S2). However, the ζ-potential of PSs remained almost constant in the presence of HA (Fig. S2). Previous study also reported that HA had little or no effect on the surface charge of PSs (Liu, Huang et al. 2020).

3.2. Aggregation behaviors of PSs

3.2.1. DBC enhanced aggregation of fresh PSs

DBC had a different refractive index, and the DLS signal was mainly derived from PSs as the solution contained more small PSs. To identify the effect mechanism of DBC on the aggregation kinetics of fresh PSs, 1, 2, and 5 mg C/L MS5, 2 mg C/L MS3, WO and RS were selected to conduct the aggregation experiments. Fig. 2 shows the change of hydrodynamic size of fresh PS_0 with time after the addition of DBC at different concentrations at several selected NaCl concentrations. As observed, all DBC appeared to increase the hydrodynamic size of fresh PSs to a certain extent under 200 mM NaCl solution. Taking MS5 as an example, with the increase in DBC concentration, the hydrodynamic size of fresh PSs increased more obviously. Particularly, after adding 5 mg C/L DBC, the particle size increased significantly to 600 nm within 30 min, while individual PS_0 maintained high stability in 200 mM NaCl solution. The SEM images reveal that PS_0 were partially connected, implying that aggregation was not obvious in this case (Fig. S6a). However, parts of the PS_0 attached to the DBC surface and clustered together (Fig. S6b) in the presence of DBC. Therefore, DBC was conducive to the aggregation of PS_0 to some extent. According to the change in the ζ-potential of the PSs in Fig. S2, the reduced electrostatic repulsion was responsible for the increased aggregation of PSs. However, when the ionic strength exceeded 400 mM, the positive effect of DBC on PSs aggregation weakened and even disappeared. The SEM images also indicated that PSs significantly aggregated in 500 mM NaCl solution compared to low ionic strength (Fig. S6c). Although DBC can form heretoaggregates with some PSs, only a minimal effect on the average aggregate size was observed (Fig. S7d). Thus, the presence of DBC is not significantly influential on the hydrodynamic size of PSs under high salt concentrations, which is attributed to the low stability of individual PSs and the limited impact of DBC.

The aggregation efficiency of PSs with or without MS5 under various salt concentrations was used to further quantify the aggregation kinetics of PSs (Fig. 3a). The initial stage when the aggregation efficiency of PSs increased with an increase in ionic strength was called the reaction-limited stage, which basically conformed to the DLVO theory (Huangfu, Ma et al. 2019, Huangfu, Xu et al. 2019, Xu, Ou et al. 2020). Under high ionic strength, the adsorption efficiency was close to 1 and remained almost constant, indicating that the energy barrier was completely shielded and the aggregation rate reached its maximum. This process is known as the diffusion-limited stage (Liu, Hu et al. 2019, Shams, Alam et al. 2020). The ionic strength corresponding to the transition from the reaction-limited stage to the diffusion-limited stage is called the CCC, which is usually used to evaluate the particle stability under different environmental conditions (Liu, Hu et al. 2019, Mao, Li et al. 2020, Shams, Alam et al. 2020). The CCC value of PSs measured in this study was approximately 585 mM NaCl, which was close to the CCC values reported in other papers (Cai, Hu et al. 2018, Liu, Hu et al. 2019, Wu, Jiang et al. 2019, Yu, Shen et al. 2019, Mao, Li et al. 2020, Shams, Alam et al. 2020). The CCC values of PSs in the presence of 1, 2 and 5 mg/L MS5 were 560 mM, 520 mM and 485 mM, respectively, which were lower than those of individual PSs (Fig. 3a). This suggests that DBC can destabilize PSs to some extent, and this destabilization ability is positively correlated with the DBC concentration. Generally, the increase in DBC concentration screened the surface charges of PSs because of the hydrophobic interaction and π-π interaction between them, as a result, DBC may act as a bridge between PSs and promote the aggregation of PSs. Some scholars also reported that the addition of a certain concentration of DBC could neutralize the surface charge and thus promote the aggregation of iron oxide colloidal particles because of the opposite charge between DBC and iron oxide col-

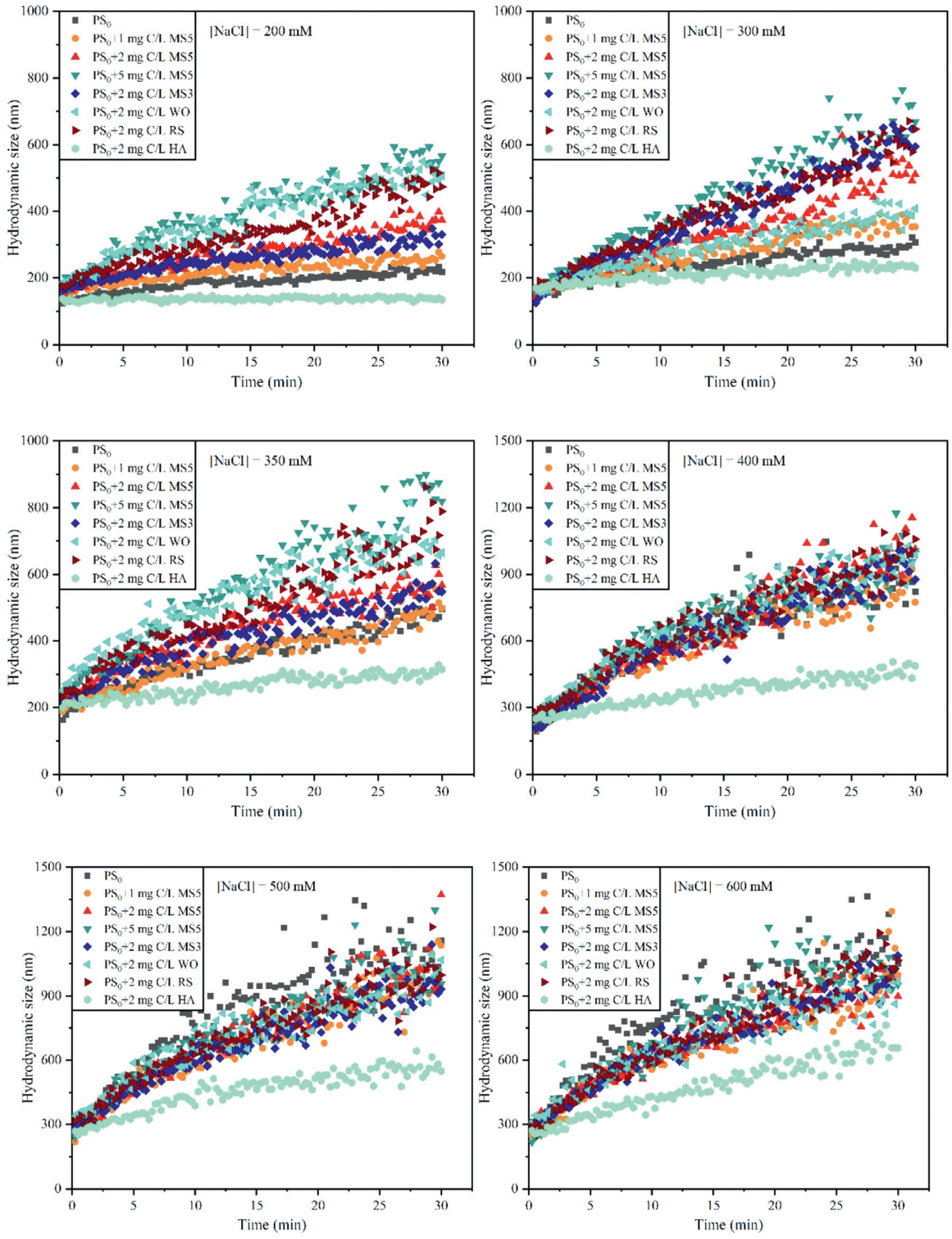

Fig. 2. Typical aggregation kinetics of PS_0 in the presence of DBC and HA as a function of NaCl concentration.

loidal particles (Lian, Yu et al. 2019). However, in this study, we found that there was a similar bridging effect, although both DBC and PSs were negatively charged.

3.2.2. Comparison of HA and different DBC

DBC is an important carbon component of DOC in aquatic environments (Armanious, Aeppli et al. 2014, Wagner, Jaffé et al. 2018, Lian, Yu et al. 2019). To distinguish the role of DBC and natural organic matter in the aggregation of nanoplastics, the aggregation kinetics of fresh PSs with 2 mg C/L MS5, MS3, WO, RS and HA were investigated. Fig. 3b shows the hydrodynamic size shift curves of PSs with 2 mg/L DBC or HA under a range of NaCl concentrations. For examples (Fig. 2), individual PS_0 and PS_0 with 2 mg C/L HA remained stable while 2 mg C/L DBC significantly increase the hydrodynamic size of PSs in 200 mM NaCl solution. This means that there was an obvious difference between DBC and HA in control-

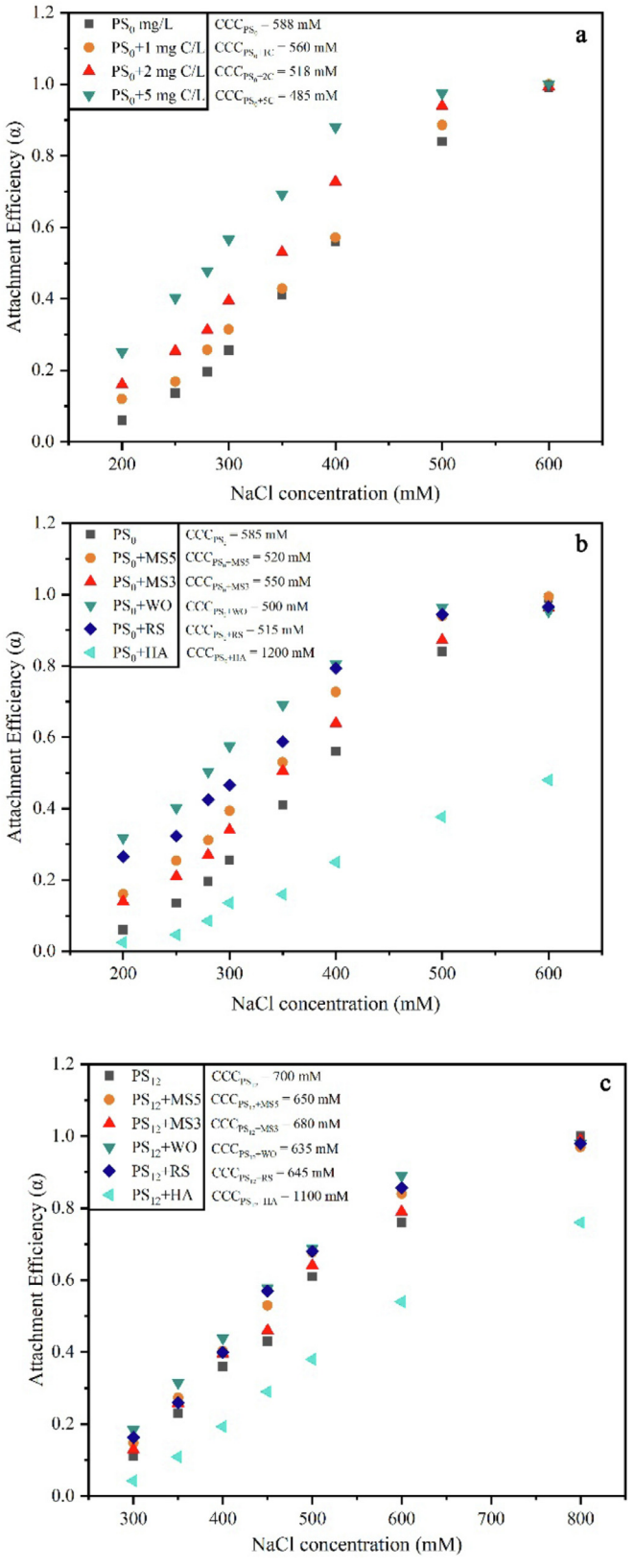

Fig. 3. Attachment efficiency of PSs as a function of NaCl concentration. (a) PS_0 with 0, 1, 2, 5 mg C/L DBC (MS5), (b) PS_0 with 2 mg/L MS5, MS3, WO, RS and HA, (c) PS_{12} with 2 mg/L MS5, MS3, WO, RS and HA.

ling the aggregation of PS_0 in NaCl solutions. Fig. 3b shows the aggregation efficiency of PS_0 with or without 2 mg/L DBC and HA at various NaCl concentrations. The CCC values of PSs in the presence of 2 mg/L MS5, MS3, WO, RS and HA were 520 mM, 550 mM, 515 mM, 500 mM, and 1200 mM, respectively. Notably, the presence of DBC promoted the aggregation of PSs, whereas HA strongly stabilized PS_0.

Additionally, the four DBC samples exhibited different extents of aggregation effects on the PS_0 in NaCl solutions. The physicochemical properties of DBC from different sources may play an important role in dominating the processes. For example, the promotion effect of MS3 produced by low-temperature pyrolysis of maize straw was the weakest, which was likely related to its higher hydrophilicity and more negative zeta potential compared with other DBC produced at high temperatures (Table S1 and Fig. S5). Thus the presence of MS3 insignificantly affected the stability of PS_0. Generally, the positive effect of DBC on PS_0 aggregation likely resulted from the electrical double-layer compression mechanism. As discussed above (Fig. S2), the presence of DBC screened the negative charges of PS_0 due to the binding of DBC. Because of the different physicochemical characteristics of different, the zeta potential of PS_0 in the presence of DBC followed WO > RS > MS5 > MS3 (Fig. S2), which is consistent with the change rule of CCC values. In contrast to DBC, the adsorption of HA on the PS_0 surface slightly changed the surface charges of PS_0 (Fig. S2), which reflects the findings of previous studies (Liu, Huang et al. 2020). Most studies implied that the HA molecules absorbed on the PS_0 surface can produce steric repulsion and therefore strongly enhance the stability of PS_0 (Liu, Huang et al. 2020, Shams, Alam et al. 2020).

3.2.3. *Effect on the aggregation of aged PSs*

As previously mentioned, hydrophobic PSs can absorb DBC and HA to varying degrees, either by promoting or inhibiting their aggregation. Environmental PSs are likely to undergo the aging process, DBC and HA may have distinct effects on the aggregation of aged PSs. Fig. S7 and S8 show the hydrodynamic size shift curves of PS_{12} and PS_{24} in the presence of 2 mg/L DBC and HA under a range of NaCl concentrations. After UV radiation, PS_{12} and PS_{24} contained more hydrophilic oxygen-containing groups that could form hydrogen bonds with water, resulting in higher stability than PS_0 (Table S1) (Cai, Hu et al. 2018, Liu, Hu et al. 2019). Notably, the hydrodynamic size of PS_{24} with and without DBC and HA barely changed even in 1000 mM NaCl solution (Fig. S8). Fig. 3c describes the aggregation efficiency of PS_{12} with or without 2 mg/L DBC and HA at various NaCl concentrations. The CCC value of PS_{12} was 700 mM NaCl, which was similar to the CCC values reported in previous studies (Liu, Hu et al. 2019, Mao, Li et al. 2020). Studies also suggested that enhanced electrostatic repulsion due to deprotonation of O-containing functional groups, as well as steric hindrance between formed molecules on aged PS surfaces, were responsible for the stability of aged PSs (Liu, Hu et al. 2019). In this study, there was no significant difference in zeta potential between aged PSs and fresh PSs (Fig. S2). Thus, the enhanced stability of aged PSs may be attributed to the enhanced hydration repulsion (Xu, Wei et al. 2017, Liu, Hu et al. 2019, Xu, Ou et al. 2020).

In addition, the effects of DBC and HA on the aggregation of aged PSs were different from those of the fresh PSs. Notably, the CCC value of PS_{12} in the presence of HA was 1100 mM, which was slightly lower than that of PS_0 in the presence of HA (Fig. 3b and 3c). Hence, the inhibitory effect of HA on the aggregation of aged PSs was not as strong. As PS_0 is more hydrophobic, it can absorb HA more easily than hydrophilic PS_{12}. The steric repulsion derived from the adsorbed HA layer was the primary mechanism of enhanced PS_0 stability (Liu, Huang et al. 2020, Shams, Alam et al. 2020). Therefore, the weak interaction between HA and aged PSs was likely responsible for the reduced inhibitory effect of HA. Similarly, while DBC promoted the aggregation of PS_{12} to some extent, the effect was not significant (Fig. S7 and 3c).

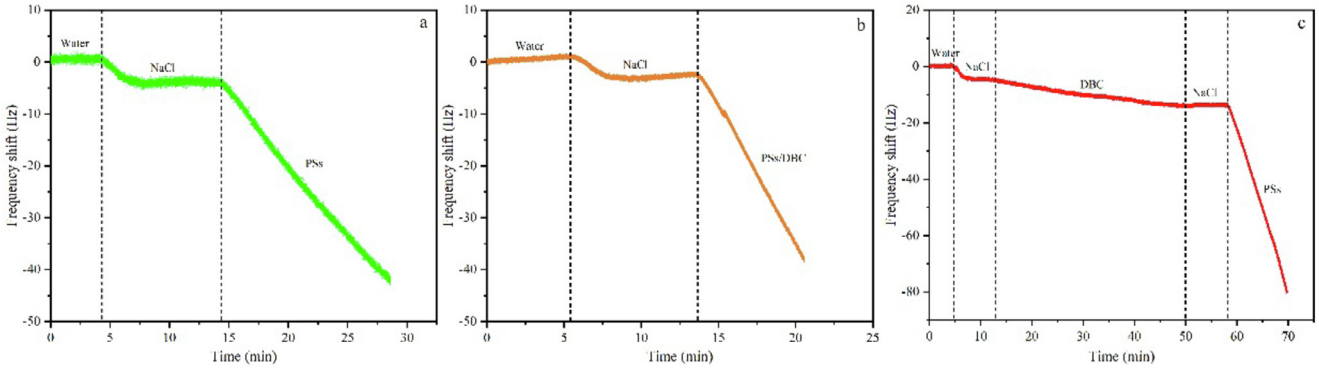

Fig. 4. (a) Representative frequency shift curve of the deposition of individual PSs on the SiO_2 surface (50 mM), (b) Representative frequency shift curve of the co-deposition of PSs and DBC on the SiO_2 surface (50 mM), (c) Representative frequency shift curve of the deposition of PSs on the SiO_2 surface coated with DBC (50 mM NaCl).

3.3. Deposition behaviors of PSs

3.3.1. Influence of DBC and HA

To explore the influence of DBC or HA on the deposition behavior of fresh PSs on environmental surface, we studied the co-deposition behavior of DBC or HA and PS_0 on a representative SiO_2 surface, as well as the deposition behavior of PS_0 on the surface of SiO_2 coated with DBC (Fig. 4). Fig. 4a and S9 show the representative frequency shift curve of individual PS_0 deposited on the silica surface (50 mM). The deposition process of PS_0 can lead to an obvious frequency shift. The initial deposition rate was 3.52 ± 0.31 Hz/min, indicating that the deposition behavior can occur under low ionic strengths. Fig. 4b and S9 represents the representative frequency shift curves of PS_0 deposited on the SiO_2 surface in the presence of 2 mg C/L DBC and HA. After adding 2 mg/L of DBC, the frequency shift was more obvious than that of individual PS_0, while the addition of HA inhibited this process. The initial deposition rates when adding MS5, MS3, WO, RS and HA were 5.84 ± 0.25, 4.05 ± 0.14, 7.23 ± 0.42, 5.45 ± 0.11, and 2.60 ± 0.10 Hz/min (Fig. 5a). Similar to the aggregation experiments, the adsorption of DBC on PS_0 surface reduced the surface charge of PS_0 (Fig. S2), resulting in a decrease the electrostatic repulsion between PS_0 and the silica surface. The promotion effect of different DBC generally followed WO > RS ≈ MS5 > MS3, which is in agreement with the zeta potential of PSs in the presence of DBC (Fig. S2). In contrast, the presence of HA prevented the deposition of PS_0 due to the additional steric repulsion. Other publications have also reported that HA can limit the deposition of several engineered nanoparticles such as MnO_2, fullerene, quantum dots, and silver nanoparticles (Qu, Alvarez et al. 2012, Furman, Usenko et al. 2013, Quevedo, Olsson et al. 2013, Huangfu, Ma et al. 2019).

The deposition process of PS_0 on the DBC-or HA-coated silica surface (Fig. 4c, and S9) was further studied to investigate the impact of DBC or HA adsorbed on the environmental surface. After pre-depositing 2 mg C/L DBC on silica surface, there was a significant frequency shift when PS_0 was added (Fig. S9). The deposition experiment can provide information about the affinity of PS_0 to the surface, and such a large deposition rate suggested there was a strong interaction between PS_0 and DBC, although both were negatively charged, which may be attributed to the strong hydrophobic and π-π interactions between PS_0 and the aromatic component of DBC. In this case, DBC deposited on surface was likely to act as a bridge, mediating the deposition of PS_0 on the silica surface. This bridging effect of DBC was similar to the DBC-mediated contact between PS_0 in the aggregation experiment (Fig. 2). Several studies have reported increased nanoparticle deposition by surface-immobilized macromolecules, including C_{60} deposition on alginate and EPS-coated silica surfaces (Chen and Elimelech 2008, Tong, Ding et al. 2010), and $nMnO_2$ on a protein (bovine serum albumin)-coated silica surface in monovalent electrolyte solutions (Huangfu, Ma et al. 2019), which was likely attributed to the hydrophobic effect of these macromolecules. In this study, the adsorption of DBC on the surface of the silica surface may provide more hydrophobic binding sites for PSs. In contrast, the coating of HA impeded PS_0 deposition due to additional steric repulsion (Qu, Alvarez et al. 2012, Furman, Usenko et al. 2013).

With the increase in NaCl concentration (e.g., 100 and 200 mM), the deposition rate of PS_0 with or without DBC and HA increased due to the decreased electrostatic repulsion (Fig. 5a and 5b) (Quevedo, Olsson et al. 2013, Xu, Ou et al. 2020). However, the cases differed with further increases in salt concentration. At high ionic strength (e.g., 500 mM), the deposition rates of both individual PS_0 and PS_0 with DBC dramatically decreased. This was attributed to the reduced mass transfer rate due to the aggregation the particles, and many publications have reported on this diffusion-limited transport mechanism (Qu, Alvarez et al. 2012, Huangfu, Ma et al. 2019, Xu, Ou et al. 2020). In the diffusion-limited stage, neither DBC in solution nor DBC adsorbed on the silica surface had any effect on the deposition of PS_0. However, at high NaCl concentrations, the initial deposition rate of PS_0 co-deposited with HA was much higher than that of individual PS_0, resulting from enhanced mass transfer rate of PS_0 in the presence of HA because of the smaller particle size (Qu, Alvarez et al. 2012). Owing to the domination of diffusion-limited transport, the absorbed HA on the silica surface had a minimal effect on the deposition of PS_0.

3.3.2. Deposition of aged PSs

The aging of PSs significantly affected their deposition. For examples, with the increase of aging time, the deposition rate of PSs in 50 mM NaCl solution dramatically reduced from 3.52 ± 0.31 Hz/min for PS_0 to 2.10 ± 0.11 Hz/min for PS_{12} and 0.98 ± 0.14 Hz/min for PS_{24} (Fig. 5c, 5e, S10 and S11). This was similar to the aggregation phenomenon that the increased hydrophilicity of PS_{12} and PS_{24} inhibited both the aggregation and deposition processes, and similar results were reported for the deposition of UVA-irradiated nC_{60} (Qu, Alvarez et al. 2012). With the increase in NaCl concentration, the initial deposition rate of PS_{12} first increased and then decreased. This was attributed to the enhanced hydrodynamic size of PS_{12}, implying that the diffusion-limited transport was also present in the deposition of PS_{12} at high salt concentration. However, the initial deposition rate of PS_{24} constantly increased from 0.98 ± 0.14 Hz/min to 3.20 ± 0.11 Hz/min as the NaCl concentration increased from 50 to 800 mM (Fig. 5e). As discussed above, PS_{24} hardly aggregated even at 1000 mM NaCl

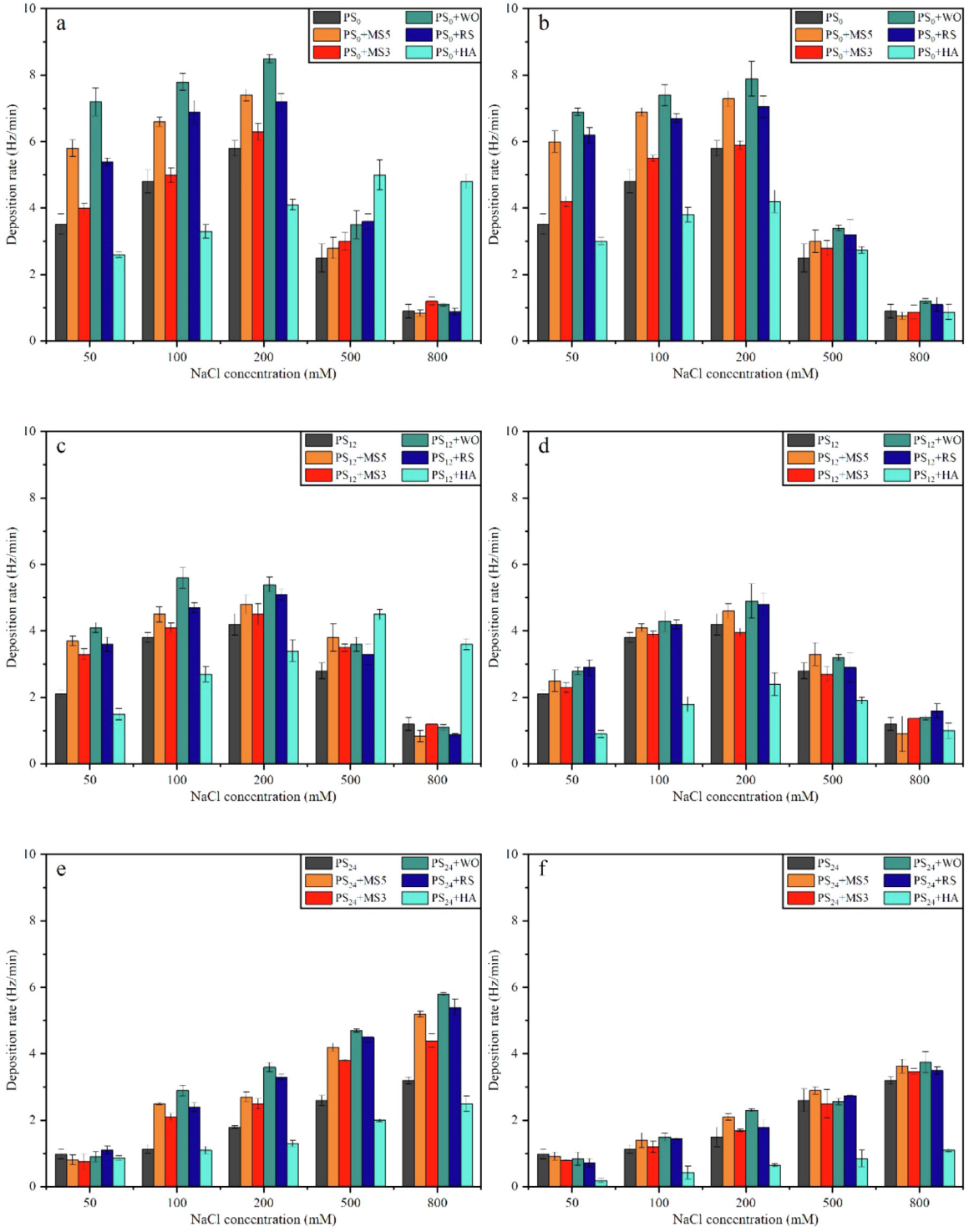

Fig. 5. The deposition rate change of fresh and aged PSs with NaCl concentration in the presence and absence of DBC and HA (2 mg/L). (a) The co-deposition of PS_0 and DBC or HA on the SiO_2 surface, (b) The deposition of PS_0 on the SiO_2 surface coated with DBC or HA, (c) The co-deposition of PS_{12} and DBC or HA on the SiO_2 surface, (d) The deposition of PS_{12} on the SiO_2 surface coated with DBC or HA, (e) The co-deposition of PS_{24} and DBC or HA on the SiO_2 surface, (f) The deposition of PS_{24} on the SiO_2 surface coated with DBC or HA.

solution and thus the electrostatic interaction rather than mass transfer rate controlled the deposition of PS_{24} (Fig. S8).

The initial deposition rates of PS_{12} and PS_{24} in the presence of DBC were higher than that of individual PS_{12} and PS_{24}, which was similar with the effect of DBC on the deposition of PS_0. Notably, the effect of DBC on the deposition of aged PSs was not as strong as that on fresh PSs due to the weak interaction between DBC and aged PSs owing to their high hydrophilicity. In particular, the deposition rates of PS_{12} and PS_{24} on the DBC-modified silica surface were insignificantly different from those on the silica surface, which indicated the limited role in controlling the deposition of aged PSs (Fig. 5d and 5f). The presence of HA in either salt solution or silica surface was not conducive to the deposition of aged PSs because of the additional steric repulsion (Fig. 5c-5f).

4. Conclusions and environmental implications

The aggregation and deposition of nanoplastics are important for evaluating their fate in aquatic environments. Current studies have focused on the aggregation behavior of PSs under different conditions, such as the effects of salt concentration and valence (Cai, Hu et al. 2018, Mao, Li et al. 2020), pH (Shams, Alam et al. 2020), aging (Liu, Hu et al. 2019, Mao, Li et al. 2020), natural organic matter and biological macromolecules (Dong, Hou et al. 2020, Leiser, Wu et al. 2020, Liu, Huang et al. 2020), temperature (Alimi, Farner et al. 2021), as well as their heteroaggregation behaviors with marine phytoplankton (Long, Paul-Pont et al. 2017), suspended sediment or natural colloids (Oriekhova and Stoll 2018, Li, Wang et al. 2019), and engineered nanoparticles (Li, He et al. 2020). These studies provide insights into the transport of nanoplastics in complex aquatic environments. DBC is an important component of DOC, accounting for approximately 10% of the DOC in rivers and 2% in oceans (Hopkinson and Vallino 2005, Dittmar and Paeng 2009, Dittmar, de Rezende et al. 2012, Rudolf Jaffé, Yan Ding et al. 2013). Elucidating the effect of DBC on the aggregation and deposition of nanoplastics is important for understanding the transport of nanoplastics in natural environments. Our study found that DBC from the four sources can promote the aggregation of PSs to some extent. The deposition experiments also showed that the coexistence of DBC promoted the deposition of PSs on the silica surface. Similarly, the DBC-modified silica surface was also conducive to PS attachment. Our findings provide new insights into the effect of DBC on the fate of environmental contaminants and enrich the research on the transport of nanoplastics in complex aquatic systems. The work on the influence of DBC and HA on the deposition process of nanoplastics on environmental surfaces is also meaningful for understanding the accumulation of fine plastic particles in river/lake sediment, as well as the potential effects of dissolved BC and natural organic matter.

This study had several limitations. For example, similar to other articles, the selected commercial PSs are unlikely to represent nanoplastics in actual aquatic environments, and the amount and distribution characteristics of nanoplastics in aquatic systems remain unknown. Additionally, as reported in previous studies and this study, commercial PSs with the critical coagulation concentration of 500-600 mM NaCl under neutral conditions are very stable; thus these works are profound only in the range of high ionic strengths and short time horizons. Studies on the fate of PSs can help predict their possible environmental behavior and potential ecological risks. Future studies should focus on the quantification and identification of nanoplastics in actual environments, and the long-term vertical or horizontal migration of nanoplastics commonly detected in the real environment requires further research.

Declaration of Competing Interest

The authors declare that they have no known competing financial interests or personal relationships that could have appeared to influence the work reported in this paper.

Acknowledgments

The present work has been financially supported by the National Natural Science Foundation of China (52070029, 51878092, 51608067), and basic scientific research operating expenses of central universities (2019CDCGHJ326). The authors appreciate the help provided by Dr. Min Wang and Biolin Scientific.

Supplementary materials

Supplementary material associated with this article can be found, in the online version, at doi:10.1016/j.watres.2021.117054.

References

Alam, M.S., Gorman-Lewis, D., Chen, N., Flynn, S.L., Ok, Y.S., Konhauser, K.O., Alessi, D.S., 2018. Thermodynamic Analysis of Nickel(II) and Zinc(II) Adsorption to Biochar. Environ Sci Technol 52 (11), 6246–6255.
Alimi, O.S., Farner Budarz, J., Hernandez, L.M., Tufenkji, N., 2018. Microplastics and Nanoplastics in Aquatic Environments: Aggregation, Deposition, and Enhanced Contaminant Transport. Environ Sci Technol 52 (4), 1704–1724.
Alimi, O.S., Farner, J.M., Tufenkji, N., 2021. Exposure of nanoplastics to freeze-thaw leads to aggregation and reduced transport in model groundwater environments. Water Res 189, 116533.
Aller, M.F., 2016. Biochar properties: Transport, fate, and impact. Critical Reviews in Environmental Science and Technology 46 (14-15), 1183–1296.
Alomar, C., Deudero, S., 2017. Evidence of microplastic ingestion in the shark Galeus melastomus Rafinesque, 1810 in the continental shelf off the western Mediterranean Sea. Environ Pollut 223, 223–229.
Armanious, A., Aeppli, M., Sander, M., 2014. Dissolved organic matter adsorption to model surfaces: adlayer formation, properties, and dynamics at the nanoscale. Environ Sci Technol 48 (16), 9420–9429.
Bergami, E., Pugnalini, S., Vannuccini, M.L., Manfra, L., Faleri, C., Savorelli, F., Dawson, K.A., Corsi, I., 2017. Long-term toxicity of surface-charged polystyrene nanoplastics to marine planktonic species Dunaliella tertiolecta and Artemia franciscana. Aquat Toxicol 189, 159–169.
Besseling, E., Foekema, E.M., Van Franeker, J.A., Leopold, M.F., Kuhn, S., Bravo Rebolledo, E.L., Hesse, E., Mielke, L., J, I.J., Kamminga, P., Koelmans, A.A., 2015. Microplastic in a macro filter feeder: Humpback whale Megaptera novaeangliae. Mar Pollut Bull 95 (1), 248–252.
Besseling, E., Quik, J.T.K., Sun, M., Koelmans, A.A., 2017. Fate of nano- and microplastic in freshwater systems: A modeling study. Environ Pollut 220 (Pt A), 540–548.
Cai, L., Hu, L., Shi, H., Ye, J., Zhang, Y., Kim, H., 2018. Effects of inorganic ions and natural organic matter on the aggregation of nanoplastics. Chemosphere 197, 142–151.
Chen, K.L., Elimelech, M., 2006. Aggregation and Deposition Kinetics of Fullerene (C60) Nanoparticles. Langmuir 22, 10994–11001.
Chen, K.L., Elimelech, M., 2008. Interaction of Fullerene (C60) Nanoparticles with Humic Acid and Alginate Coated Silica Surfaces: Measurements, Mechanisms, and Environmental Implications. Environmental science & technology 24, 7607–7614.
Chua, E.M., Shimeta, J., Nugegoda, D., Morrison, P.D., Clarke, B.O., 2014. Assimilation of polybrominated diphenyl ethers from microplastics by the marine amphipod, Allorchestes compressa. Environ Sci Technol 48 (14), 8127–8134.
Cole, M., Lindeque, P.K., Fileman, E., Clark, J., Lewis, C., Halsband, C., Galloway, T.S., 2016. Microplastics Alter the Properties and Sinking Rates of Zooplankton Faecal Pellets. Environ Sci Technol 50 (6), 3239–3246.
Ding, Y., Cawley, K.M., da Cunha, C.N., Jaffé, R., 2014. Environmental dynamics of dissolved black carbon in wetlands. Biogeochemistry.
Dittmar, T., de Rezende, C.E., Manecki, M., Niggemann, J., Coelho Ovalle, A.R., Stubbins, A., Bernardes, M.C., 2012. Continuous flux of dissolved black carbon from a vanished tropical forest biome. Nature Geoscience 5 (9), 618–622.
Dittmar, T., Paeng, J., 2009. A heat-induced molecular signature in marine dissolved organic matter. Nature Geoscience 2 (3), 175–179.
Dong, Z., Hou, Y., Han, W., Liu, M., Wang, J., Qiu, Y., 2020. Protein corona-mediated transport of nanoplastics in seawater-saturated porous media. Water Res 182, 115978.
Eerkes-Medrano, D., Thompson, R.C., Aldridge, D.C., 2015. Microplastics in freshwater systems: a review of the emerging threats, identification of knowledge gaps and prioritisation of research needs. Water Res 75, 63–82.
Enfrin, M., Dumee, L.F., Lee, J., 2019. Nano/microplastics in water and wastewater treatment processes - Origin, impact and potential solutions. Water Res 161, 621–638.
Erni-Cassola, G., Gibson, M.I., Thompson, R.C., Christie-Oleza, J.A., 2017. Lost, but Found with Nile Red: A Novel Method for Detecting and Quantifying Small Microplastics (1 mm to 20 um) in Environmental Samples. Environ Sci Technol 51 (23), 13641–13648.
Furman, O., Usenko, S., Lau, B.L., 2013. Relative importance of the humic and fulvic fractions of natural organic matter in the aggregation and deposition of silver nanoparticles. Environ Sci Technol 47 (3), 1349–1356.
Harvey, O.R., Herbert, B.E., Rhue, R.D., Kuo, L.J., 2011. Metal interactions at the biochar-water interface: energetics and structure-sorption relationships elucidated by flow adsorption microcalorimetry. Environ Sci Technol 45 (13), 5550–5556.
Hopkinson, C.S., Vallino, J.J., 2005. Efficient export of carbon to the deep ocean through dissolved organic matter. Nature 433 (7022), 142–145.
Huangfu, X., Ma, C., Huang, R., He, Q., Liu, C., Zhou, J., Jiang, J., Ma, J., Zhu, Y., Huang, M., 2019. Deposition Kinetics of Colloidal Manganese Dioxide onto Representative Surfaces in Aquatic Environments: The Role of Humic Acid and Biomacromolecules. Environ Sci Technol 53 (1), 146–156.

Huangfu, X., Xu, Y., Liu, C., He, Q., Ma, J., Ma, C., Huang, R., 2019. A review on the interactions between engineered nanoparticles with extracellular and intracellular polymeric substances from wastewater treatment aggregates. Chemosphere 219, 766–783.
Huffer, T., Hofmann, T., 2016. Sorption of non-polar organic compounds by micro–sized plastic particles in aqueous solution. Environ Pollut 214, 194–201.
Jiang, Y., Raliya, R., Fortner, J.D., Biswas, P., 2016. Graphene Oxides in Water: Correlating Morphology and Surface Chemistry with Aggregation Behavior. Environ Sci Technol 50 (13), 6964–6973.
Leiser, R., Wu, G.M., Neu, T.R., Wendt-Potthoff, K., 2020. Biofouling, metal sorption and aggregation are related to sinking of microplastics in a stratified reservoir. Water Res 176, 115748.
Li, X., He, E., Xia, B., Van Gestel, C.A.M., Peijnenburg, W., Cao, X., Qiu, H., 2020. Impact of CeO2 nanoparticles on the aggregation kinetics and stability of polystyrene nanoplastics: Importance of surface functionalization and solution chemistry. Water Res 186, 116324.
Li, Y., Wang, X., Fu, W., Xia, X., Liu, C., Min, J., Zhang, W., Crittenden, J.C., 2019. Interactions between nano/micro plastics and suspended sediment in water: Implications on aggregation and settling. Water Res 161, 486–495.
Lian, F., Xing, B., 2017. Black Carbon (Biochar) In Water/Soil Environments: Molecular Structure, Sorption, Stability, and Potential Risk. Environ Sci Technol 51 (23), 13517–13532.
Lian, F., Yu, W., Wang, Z., Xing, B., 2019. New Insights into Black Carbon Nanoparticle-Induced Dispersibility of Goethite Colloids and Configuration-Dependent Sorption for Phenanthrene. Environ Sci Technol 53 (2), 661–670.
Liu, J., Legros, S., von der Kammer, F., Hofmann, T., 2013. Natural organic matter concentration and hydrochemistry influence aggregation kinetics of functionalized engineered nanoparticles. Environ Sci Technol 47 (9), 4113–4120.
Liu, J., Ma, Y., Zhu, D., Xia, T., Qi, Y., Yao, Y., Guo, X., Ji, R., Chen, W., 2018. Polystyrene Nanoplastics-Enhanced Contaminant Transport: Role of Irreversible Adsorption in Glassy Polymeric Domain. Environ Sci Technol 52 (5), 2677–2685.
Liu, L., Fokkink, R., Koelmans, A.A., 2016. Sorption of polycyclic aromatic hydrocarbons to polystyrene nanoplastic. Environ Toxicol Chem 35 (7), 1650–1655.
Liu, Y., Hu, Y., Yang, C., Chen, C., Huang, W., Dang, Z., 2019. Aggregation kinetics of UV irradiated nanoplastics in aquatic environments. Water Res 163, 114870.
Liu, Y., Huang, Z., Zhou, J., Tang, J., Yang, C., Chen, C., Huang, W., Dang, Z., 2020. Influence of environmental and biological macromolecules on aggregation kinetics of nanoplastics in aquatic systems. Water Res 186, 116316.
Long, M., Paul-Pont, I., Hegaret, H., Moriceau, B., Lambert, C., Huvet, A., Soudant, P., 2017. Interactions between polystyrene microplastics and marine phytoplankton lead to species-specific hetero-aggregation. Environ Pollut 228, 454–463.
Luo, L., Chen, Z., Lv, J., Cheng, Y., Wu, T., Huang, R., 2019. Molecular understanding of dissolved black carbon sorption in soil-water environment. Water Res 154, 210–216.
Luo, L., Xu, C., Chen, Z., Zhang, S., 2015. Properties of biomass-derived biochars: Combined effects of operating conditions and biomass types. Bioresource Technology 192, 83–89.
Mao, Y., Ai, H., Chen, Y., Zhang, Z., Zeng, P., Kang, L., Li, W., Gu, W., He, Q., Li, H., 2018. Phytoplankton response to polystyrene microplastics: Perspective from an entire growth period. Chemosphere 208, 59–68.
Mao, Y., Li, H., Huangfu, X., Liu, Y., He, Q., 2020. Nanoplastics display strong stability in aqueous environments: Insights from aggregation behaviour and theoretical calculations. Environ Pollut 258, 113760.
Oriekhova, O., Stoll, S., 2018. Heteroaggregation of nanoplastic particles in the presence of inorganic colloids and natural organic matter. Environmental Science: Nano 5 (3), 792–799.
Ouyang, W., Zhao, X., Tysklind, M., Hao, F., 2016. Typical agricultural diffuse herbicide sorption with agricultural waste-derived biochars amended soil of high organic matter content. Water Res 92, 156–163.
Qian, L., Zhang, W., Yan, J., Han, L., Gao, W., Liu, R., Chen, M., 2016. Effective removal of heavy metal by biochar colloids under different pyrolysis temperatures. Bioresour Technol 206, 217–224.
Qu, X., Alvarez, P.J., Li, Q., 2012. Impact of sunlight and humic acid on the deposition kinetics of aqueous fullerene nanoparticles (nC60). Environ Sci Technol 46 (24), 13455–13462.
Qu, X., Fu, H., Mao, J., Ran, Y., Zhang, D., Zhu, D., 2016. Chemical and structural properties of dissolved black carbon released from biochars. Carbon 96, 759–767.
Quevedo, I.R., Olsson, A.L., Tufenkji, N., 2013. Deposition kinetics of quantum dots and polystyrene latex nanoparticles onto alumina: role of water chemistry and particle coating. Environ Sci Technol 47 (5), 2212–2220.
Rudolf, Jaffé, Ding, Yan, Niggemann, Jutta, Vähätalo, Anssi V., Stubbins, Aron, Spencer, Robert G.M., John Campbell, T.D., 2013. Global charcoal mobilization from soils via dissolution and riverine transport to the oceans. Science 340 (6130), 345–347.
Shams, M., Alam, I., Chowdhury, I., 2020. Aggregation and stability of nanoscale plastics in aquatic environment. Water Res 171, 115401.
Summers, S., Henry, T., Gutierrez, T., 2018. Agglomeration of nano- and microplastic particles in seawater by autochthonous and de novo-produced sources of exopolymeric substances. Mar Pollut Bull 130, 258–267.
Tong, M., Ding, J., Shen, Y., Zhu, P., 2010. Influence of biofilm on the transport of fullerene (C60) nanoparticles in porous media. Water Research 44 (4), 1094–1103.
Velzeboer, I., Kwadijk, C.J., Koelmans, A.A., 2014. Strong sorption of PCBs to nanoplastics, microplastics, carbon nanotubes, and fullerenes. Environ Sci Technol 48 (9), 4869–4876.
Wagner, S., Jaffé, R., Stubbins, A., 2018. Dissolved black carbon in aquatic ecosystems. Limnology and Oceanography Letters 3 (3), 168–185.
Wang, J., Zhao, X., Wu, A., Tang, Z., Niu, L., Wu, F., Wang, F., Zhao, T., Fu, Z., 2021. Aggregation and stability of sulfate-modified polystyrene nanoplastics in synthetic and natural waters. Environ Pollut 268 (Pt A), 114240.
Wu, J., Jiang, R., Lin, W., Ouyang, G., 2019. Effect of salinity and humic acid on the aggregation and toxicity of polystyrene nanoplastics with different functional groups and charges. Environ Pollut 245, 836–843.
Xu, C., Xue, Y., Qi, Y., Wang, X., 2016. Quantities and Fluxes of Dissolved and Particulate Black Carbon in the Changjiang and Huanghe Rivers, China. Estuaries and Coasts 39 (6), 1617–1625.
Xu, F., Wei, C., Zeng, Q., Li, X., Alvarez, P.J.J., Li, Q., Qu, X., Zhu, D., 2017. Aggregation Behavior of Dissolved Black Carbon: Implications for Vertical Mass Flux and Fractionation in Aquatic Systems. Environ Sci Technol 51 (23), 13723–13732.
Xu, Y., He, Q., Liu, C., Huangfu, X., 2019. Are Micro- or Nanoplastics Leached from Drinking Water Distribution Systems? Environ Sci Technol 53 (16), 9339–9340.
Xu, Y., Ou, Q., Liu, C., Zhou, X., He, Q., Wu, Z., Huang, R., Ma, J., Lu, D., Huangfu, X., 2020. Aggregation and deposition behaviors of dissolved black carbon with coexisting heavy metals in aquatic solution. Environmental Science: Nano.
Yao, Y., Gao, B., Fang, J., Zhang, M., Chen, H., Zhou, Y., Creamer, A.E., Sun, Y., Yang, L., 2014. Characterization and environmental applications of clay–biochar composites. Chemical Engineering Journal 242, 136–143.
Yu, S., Shen, M., Li, S., Fu, Y., Zhang, D., Liu, H., Liu, J., 2019. Aggregation kinetics of different surface-modified polystyrene nanoparticles in monovalent and divalent electrolytes. Environ Pollut 255 (Pt 2), 113302.